AEM
Journals.ASM.org

Dynamic Mechanisms of the Bactericidal Action of an Al_2O_3-TiO_2-Ag Granular Material on an *Escherichia coli* Strain

Marie-Anne Tartanson,[a,b] Laurence Soussan,[a] Matthieu Rivallin,[a] Sophie Pecastaings,[c] Cristian V. Chis,[b] Diego Penaranda,[b] Christine Roques,[c] Catherine Faur[a]

Institut Européen des Membranes (IEM) (UMR 5635 CNRS-ENSCM-UM2)-Equipe Génie des Procédés Membranaires, Université Montpellier, Montpellier, France[a]; CARDPool SAS, Research and Development Site, Alès, France[b]; Université de Toulouse, UPS, Laboratoire de Génie Chimique, BioSym Dpt. UMR 5503, Faculté de Pharmacie, Toulouse, France[c]

The bactericidal activity of an Al_2O_3-TiO_2-Ag granular material against an *Escherichia coli* strain was confirmed by a culture-based method. In particular, 100% of microorganisms were permanently inactivated in 30 to 45 min. The present work aimed to investigate the mechanisms of the bactericidal action of this material and their dynamics on *Escherichia coli* using different techniques. Observations by transmission electron microscopy (TEM) at different times of disinfection revealed morphological changes in the bacteria as soon as they were put in contact with the material. Notably highlighted were cell membrane damage; cytoplasm detachment; formation of vacuoles, possibly due to DNA condensation, in association with regions exhibiting different levels of electron density; and membrane lysis. PCR and flow cytometry analyses were used to confirm and quantify the observations of cell integrity. The direct exposure of cells to silver, combined with the oxidative stress induced by the reactive oxygen species (ROS) generated, was identified to be responsible for these morphological alterations. From the first 5 min of treatment with the Al_2O_3-TiO_2-Ag material, 98% of *E. coli* isolates were lysed. From 30 min, cell viability decreased to reach total inactivation, although approximately 1% of permeable *E. coli* cells and 1% of intact cells (10^5 genomic units · ml^{-1}) were evidenced. This study demonstrates that the bactericidal effect of the material results from a synergic action of desorbed and supported silver. Supported silver was shown to generate the ROS evidenced.

Traditional disinfection methods for spa waters are based on the addition of chemicals, such as chlorine (Cl) or bromine (Br), into the water. The use of ozonators or UV light reactors to reduce the amount of chemicals in water has gained considerable attention in recent decades. However, these techniques are costly and present potential dangers to human health and the environment (1). Like many inorganic compounds, silver presents interesting biocidal properties that have resulted in its widespread application in the medical (2), textile (3), and water treatment (4) fields. However, the silver content in solution is subject to safety regulations. While there is currently no standard for silver concentrations in bathing water, the U.S. Environmental Protection Agency recommends a silver concentration of less than 0.1 mg · $liter^{-1}$ in drinking water (5). To ensure that the silver concentration in drinking water is low, some researchers have developed supported silver materials, usually using zeolite or alumina supports. An important characteristic of these materials is that they inactivate the microorganisms by combining the action of supported and desorbed silver while limiting silver desorption from the material. Matsumura et al. (6) and De la Rosa-Gomez et al. (7) demonstrated the removal of *Escherichia coli* (2×10^7 CFU · ml^{-1}), while only 0.1 mg · $liter^{-1}$ of silver was desorbed from silver supported on zeolite. A similar efficiency of removal was obtained by Chen et al. (8) with silver supported on alumina.

The bactericidal effect of supported silver materials has been thoroughly investigated, and reports highlight different kinds of bactericidal action depending on the cytotoxicity of the forms of silverused: silver nanoparticles (suspended or supported), ionic silver, and supported silver. Silver nanoparticles have been reported to create pits in the cell wall, leading to unregulated transport through the cell membrane and even to the entrance of nanoparticles into the cells (9, 10). Both the nanoparticles and silver ions that enter cells were reported to be able to interfere with DNA. It is expected that the DNA molecule then conglomerates in order to protect itself from the silver attack, triggering the loss of its replication ability (11). Ionic silver was shown to strongly interact with the thiol (—SH) groups of proteins to form S-Ag, which could lead to the inactivation of respiratory chain dehydrogenases and, consequently, to a collapse of the proton gradient (12, 13). This effect could thus result in the collapse of the membrane structure and then to cell death (11, 14, 15). Finally, the production of reactive oxygen species (ROS) by the surface of supported silver material or silver nanoparticles under aerobic conditions is commonly accepted (8, 16–18). On the contrary, it seems that the intracellular generation of ROS by ionic silver is still controversial (19). These very oxidizing ROS species (such as $O_2^{-\cdot}$, H_2O_2, or $OH^{\cdot}$), which exhibit short lifetimes, could attack the cell membrane and/or intracellular components (DNA, proteins).

Among previous works carried out using supported silver, very

Received 10 June 2015 **Accepted** 20 July 2015

Accepted manuscript posted online 7 August 2015

Citation Tartanson M-A, Soussan L, Rivallin M, Pecastaings S, Chis CV, Penaranda D, Roques C, Faur C. 2015. Dynamic mechanisms of the bactericidal action of an Al_2O_3-TiO_2-Ag granular material on an *Escherichia coli* strain. Appl Environ Microbiol 81:7135–7142. doi:10.1128/AEM.01950-15.

Editor: S.-J. Liu

Address correspondence to Laurence Soussan, Laurence.Soussan@iemm.univ-montp2.fr.

Copyright © 2015, American Society for Microbiology. All Rights Reserved.

doi:10.1128/AEM.01950-15

few studies have concerned alumina supports (8, 16). The company CARDPool SAS developed an innovative macrogranular material consisting of an alumina support treated with a double layer successively made up of titanium dioxide (TiO_2) and silver (Ag) (20) in which the TiO_2 coating enabled the silver to become strongly bound to the alumina, thus limiting silver desorption (21).

Moreover, it has been demonstrated that this new material, Al_2O_3-TiO_2-Ag, has bactericidal properties against a mixture of *Escherichia coli* and *Staphylococcus epidermidis* bacteria in static and in dynamic configurations. Its antimicrobial effect was highlighted while evaluating the influence of key operating factors specific to the disinfection of spa waters (21).

In the present work, the disinfecting abilities of Al_2O_3-TiO_2-Ag were studied with the aim of correlating the dynamic inactivation of bacteria with (i) ROS generation and (ii) silver desorption in solution. Bacterial characterizations (by transmission electron microscopy [TEM], flow cytometry, and PCR analysis) were also performed during disinfection to monitor the morphological and structural changes of the cells. In order to facilitate the biomolecular analyses, the disinfectant properties were evaluated by considering only *E. coli* in this study.

MATERIALS AND METHODS

Material. Samples of the Al_2O_3-TiO_2-Ag material were synthesized using activated alumina supports (form, extruded trilobite 10 ± 1 mm in length and 1.6 ± 0.2 mm in diameter; specific area, 271 $m^2 \cdot g^{-1}$) modified by the use of two nanocoatings, one of titanium dioxide (TiO_2) and one of silver (Ag), followed by calcination (20). The first layer, TiO_2, was deposited by a specific chemical vapor deposition molecular layered (CVDML) method using titanium chloride ($TiCl_4$) as a precursor. The second layer, Ag nanoaggregates, was then deposited on the surface of the Al_2O_3-TiO_2 support by a dry impregnation method using silver nitrate salt ($AgNO_3$) as a precursor. Samples of the Al_2O_3-TiO_2-Ag material contained approximately 3% (wt/wt) TiO_2 and 7% (wt/wt) silver.

Cultivation of bacteria, preparation of bacterial suspensions, and counting of cells. A nonpathogenic *Escherichia coli* strain (K-12 DSM 423 from DSMZ, Germany) was chosen as a microorganism surrogate for microbial contamination. Cultivation and preparation of the bacterial suspensions in spring water were carried out as detailed by Tartanson et al. (21). The bacteria were counted by the conventional plaque assay method (21), which enumerates cultivable cells only, on Tergitol medium plates. Plaque assays were performed in triplicate, and the detection threshold was 8 CFU · ml^{-1}.

This method allowed the cultivable bacterial concentration in the suspensions under study to be monitored and correlated with the bactericidal performance of the material. When no bacteria were enumerated on the plates, the corresponding logarithmic value was fixed to 0 by convention.

Study of the bactericidal performance of the Al_2O_3-TiO_2-Ag material. The material (16 g · $liter^{-1}$) was immersed in a 1-liter batch reactor (with a breathable seal) containing 350 ml of seeded spring water. An *E. coli* suspension was inoculated at a final concentration of $1.0 \times 10^8 \pm 0.2 \times 10^8$ CFU · ml^{-1}, and the reactor was incubated at 22 ± 0.1°C with constant stirring (80 rpm) on a rotary shaker (21). Water samples were taken at defined times over 1 h in order to follow and characterize the kinetics of bacterial inactivation. To determine the initial bacterial concentration, sampling was always performed before the introduction of the material. These experiments were carried out under sterile conditions and without addition of nutrients. A control test (with bacteria without the test material under the same operating conditions described above) was run for each kinetic assay.

In order to check whether bacterial regrowth could occur after total *E. coli* inactivation, water samples were collected after 60 min and centrifuged to remove any traces of silver. The bacterial pellets recovered were resuspended in fresh culture medium and incubated at 37°C with constant stirring (110 rpm). After 1 h of incubation, the suspension was spread on nutrient culture dishes and incubated for 24 h at 37°C.

Each kinetic assay was performed twice.

Physicochemical characterizations. (i) Silver desorption. The change of the silver concentration in solution with time was followed to study the influence of silver desorption on the bactericidal activity of the material. Each sample was acidified with 2.5% HNO_3 to stabilize the desorbed silver, and the silver concentration was measured by atomic absorption spectroscopy (AAS; PerkinElmer). The silver concentrations of all the replicates were measured.

(ii) ROS generation. In order to assess the generation of ROS that could contribute to disinfection, the ROS free radical concentration was quantified with an OxiSelect *in vitro* ROS/reactive nitrogen species (RNS) assay kit (catalog number STA-347; Cell Biolabs, Inc.). This method analyzed the total concentration of free radicals (corresponding to extracellular ROS) in a sample; intracellular ROS were not measured. The assay employs a proprietary quenched fluorogenic probe, dichlorodihydrofluorescein (DCFH)-DiOxyGEN (DiOxyQ), which is an ROS/RNS-specific probe whose chemistry is similar to that of the popular probe 2′,7′-dichlorodihydrofluorescein (DCF) diacetate. The DCFH-DiOxyQ probe is first primed with a quench removal reagent and subsequently stabilized in the highly reactive DCFH form. In this state, ROS and RNS species can react with DCFH, which is rapidly oxidized to the highly fluorescent DCF. Fluorescence intensity is proportional to the total ROS/RNS level within the sample (H_2O_2, $ROO^{\cdot}$, NO, NOO^-). All samples and calibration curves were prepared according to the instructions of the supplier (catalog number STA-347; Cell Biolabs, Inc.). The assay was performed in a 96-well fluorescent plate format that could be read on a standard fluorescent plate reader. The free radical content in samples was determined by comparison with the predetermined DCF or hydrogen peroxide concentrations on the standard curve. Each measurement was independently reproduced twice.

Bacterial characterizations. In addition to the counting of cultivable cells, three other bacterial characterizations were carried out.

(i) TEM sample preparation and analysis. Samples were fixed with 2.5% glutaraldehyde in 0.1 M phosphate buffer (pH 7) overnight at 4°C, rinsed twice for 5 min each time in phosphate buffer, and postfixed in osmium tetroxide in 0.1 M phosphate buffer. Then, the glutaraldehyde was removed by washing three times in water and the dehydration process was conducted with 70, 90, and 100% alcohol. Fixed cells were embedded with Epon 812. Polymerization was performed at 60°C for 3 days. Blocks of Epon with bacteria (70 nm thick) were cut with an ultramicrotome (Ultracut UTC; Leica) and recovered on copper grids. The ultrathin sections were stained with uranyl acetate and lead citrate before observation by TEM with a JEOL 1200EXII TEM.

(ii) Cellular integrity (vPCR and qPCR quantifications). To quantify DNA by viability PCR (vPCR) or quantitative PCR (qPCR) during the disinfection kinetics assay, 1 ml of sample was taken from the reactor at different time points and centrifuged at 4,500 rpm for 5 min at 12°C. The bacterial pellets were mixed with 0.5 ml of distilled water. Then, DNA was extracted by means of a QIAamp DNA kit (Qiagen, France) according to the manufacturer's instructions (preliminary step before qPCR). Before the vPCR, this suspension was first incubated with 10 μg · ml^{-1} ethidium monoazide (EMA; Life Technologies, France) for 5 min in the dark at ambient temperature and then for 15 min under a neon light (11 W, phase difference $\varphi = 0.37$) on ice. The latter step allowed covalent bonds to form between EMA and extracellular DNA (and the DNA contained in damaged bacteria) in order to inhibit amplification during the PCR. The qPCRs were performed in a total volume of 25 μl including 5 μl of DNA matrix and 12.5 μl of 2× iQ SYBR green Supermix (containing iTaq polymerase, SYBR green fluorochrome, deoxynucleoside triphosphates, and enzyme buffer; Bio-Rad, France). The final concentration of each primer (primers 1080γF and γ1202R) was 350 nM. After a 5-min DNA denaturation step at 95°C, 40 cycles of PCR (95°C for 15 s, 60°C for 30 s,

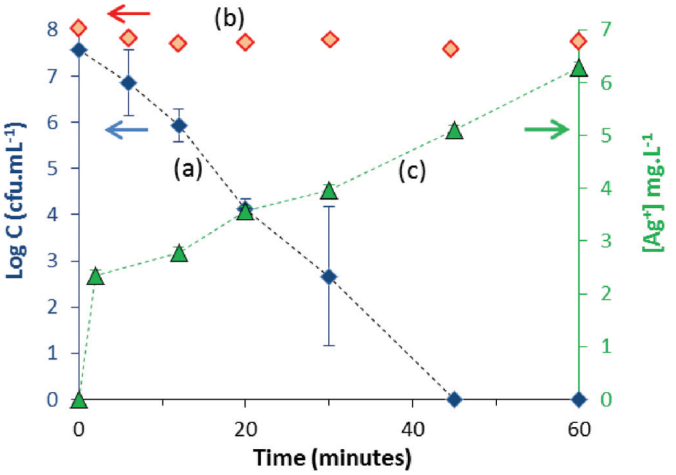

FIG 1 Kinetics of *E. coli* removal by Al_2O_3-TiO_2-Ag (16 g · liter^{-1}) (curve a), control kinetics for *E. coli* cells not treated with Al_2O_3-TiO_2-Ag (curve b), and silver desorption (curve c). The initial concentration of *E. coli* cells was $1.0 \times 10^8 \pm 0.2 \times 10^8$ CFU · ml^{-1}, and the temperature was 22°C. C, cell count.

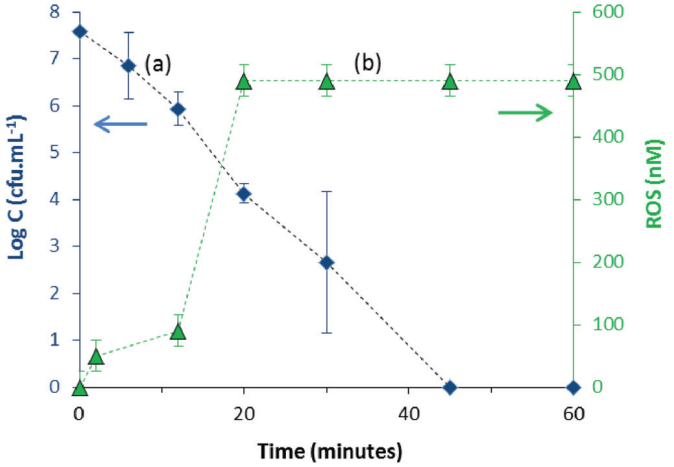

FIG 2 *E. coli* removal by 16 g · liter^{-1} of Al_2O_3-TiO_2-Ag (curve a) and kinetics of ROS generation (in nanomolar, i.e., nanomoles · liter^{-1}) (curve b). The initial concentration was $1.0 \times 10^8 \pm 0.2 \times 10^8$ CFU · ml^{-1}, and the temperature was 22°C. C, cell count.

72°C for 30 s) were performed on a MyiQ thermal cycler (Bio-Rad, France). PCR was followed by a melt curve analysis from 55°C to 95°C with an increase of 0.5°C every 10 s in order to check for the absence of contamination and primer dimers. The qPCR and vPCR methods were validated previously (data not shown), and the limit of detection corresponds to a bacterial concentration of 10^3 genomic units (GU) · ml^{-1}. Each kinetic assay was independently performed three times.

(iii) Cell permeability (flow cytometry). A LIVE/DEAD BacLight bacterial viability kit (catalog number L13152; Molecular Probes) was used to determine the relative proportion of nonpermeable intact cells and permeable cells still having a cellular membrane. With an appropriate mixture of SYTO9 green fluorescent nucleic acid stain and red fluorescent nucleic acid stain (propidium iodide), bacteria with intact membranes (usually called "live bacteria") appear fluorescent green, whereas bacteria with damaged membranes (commonly called "dead bacteria") appear fluorescent red. The excitation and emission maxima for these stains were 480 and 500 nm, respectively, for the SYTO9 stain and 490 and 635 nm, respectively, for propidium iodide. To determine the ratio of intact bacteria to bacteria with membranes damaged during the disinfection kinetics assay, 10 ml of sample was centrifuged at 4,500 × *g* for 10 min at 12°C, and the bacterial pellet was resuspended in 4 ml of 0.9% NaCl. SYTO9 (0.5 ml) and propidium iodide (0.5 ml) were added to each 1-ml sample. After 1 h of incubation in the dark at room temperature with mixing every 15 min, fluorescence measurements were carried out using a Gallios flow cytometer (Beckman Coulter, Inc.). The green fluorescence and red fluorescence in the sample were measured simultaneously by two detectors. Each analysis was performed twice. Controls were performed to check that the fluorescence signals for live bacteria and dead bacteria (green and red, respectively) were consistent with the physiological state of the bacteria. For live bacteria, 1 ml of a fresh bacterial suspension at 10^6 CFU · ml^{-1} was added to 3 ml of 0.9% NaCl, and 1 ml of the resulting solution was then mixed with 0.5 ml of SYTO9 and 0.5 ml of water. For dead bacteria, 1 ml of a fresh bacterial suspension at 10^6 CFU · ml^{-1} was added to 3 ml of 70% isopropyl alcohol, and 1 ml of the resulting solution was then mixed with 0.5 ml of propidium iodide and 0.5 ml of water. The range of bacterial concentrations analyzed was 10^3 to 10^8 CFU · ml^{-1}.

RESULTS

Bactericidal activity of the Al_2O_3-TiO_2-Ag material against *E. coli*. Figure 1 (curve a) once again confirms the bactericidal activity of the material studied, showing the total removal of cultivable *E. coli* from 45 min onwards. As early as 12 min, i.e., after a very short time of treatment, 99% of the bacterial population was inactivated. A control performed without the material showed a constant bacterial concentration (Fig. 1, curve b).

Moreover, additional tests revealed that no regrowth of bacteria was observed after the disinfection treatment. The Al_2O_3-TiO_2-Ag material thus revealed its strong bactericidal activity by permanently inactivating all bacteria, as no bacteria were cultivable at the end of the treatment.

Physicochemical characterization of species involved in disinfection. (i) Desorbed silver. It has been demonstrated that the bactericidal activity of the Al_2O_3-TiO_2-Ag material is based on both supported and desorbed silver (21). Although the TiO_2 layer of the material was shown to considerably limit silver desorption (21), silver desorption occurred as described by curve c of Fig. 1, which presents the kinetics of silver desorption: 6.5 mg · liter^{-1} of desorbed silver was obtained after 60 min of treatment with the material. Nevertheless, it is worth noting that the total desorption quantified corresponded to less than 1% of the total silver deposited on the Al_2O_3-TiO_2-Ag material (21). The kinetics of desorbed silver thus confirmed its presence, which is likely to have contributed to the inactivation of *E. coli*.

(ii) *In vitro* ROS. The presence of ROS was thus assayed during the bacterial removal kinetics assay. Figure 2 reports the curves for bacterial removal (curve a) and the change of the ROS concentration (curve b) versus time during the disinfection. ROS were present as early as the beginning of the treatment. The ROS concentration reached a maximum (about 500 nM) at 20 min and remained constant up to 60 min, while bacterial removal continued to decrease from 20 to 60 min. This result suggests either that an extracellular ROS concentration of less than 500 nM is not sufficient to inactivate all bacteria or requires a longer contact time with the cells or that the bactericidal action of ROS is coupled with another contribution of desorbed and/or supported silver. The ROS assays also revealed (data not shown) that bacteria, the material, and the desorbed silver alone did not lead to the formation of ROS. Moreover, the presence of both desorbed silver and bacteria did not lead to ROS generation. These results show that ROS

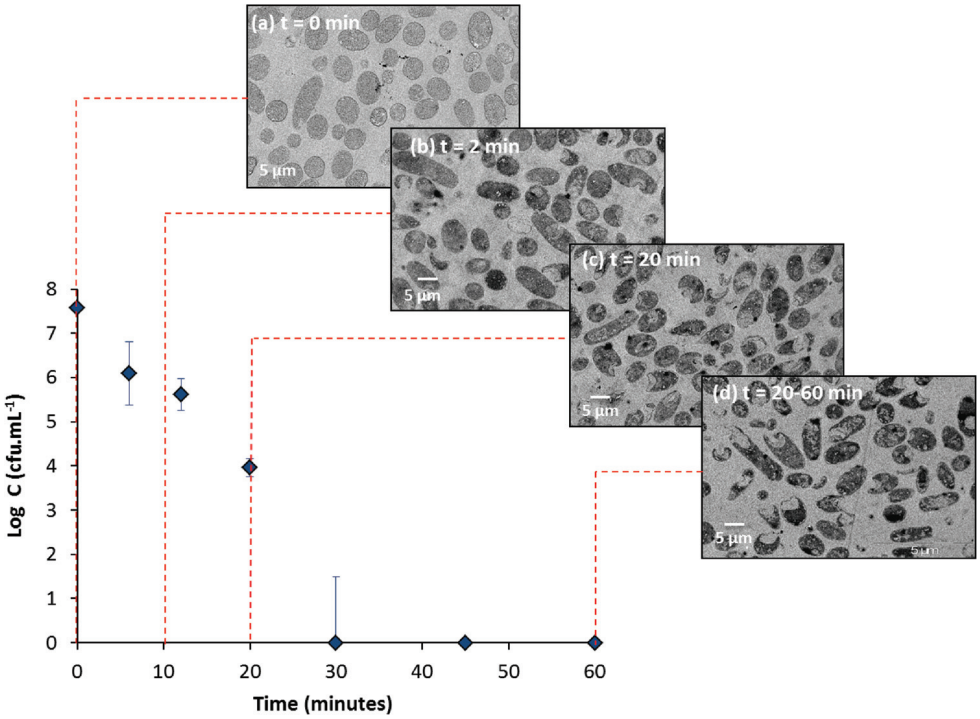

FIG 3 TEM micrographs of untreated *E. coli* cells (a), *E. coli* cells after 2 min of treatment with Al_2O_3-TiO_2-Ag (b), *E. coli* cells after 20 min of treatment with Al_2O_3-TiO_2-Ag (c), and *E. coli* cells after 60 min of treatment with Al_2O_3-TiO_2-Ag (d). The concentration of Al_2O_3-TiO_2-Ag was 16 g · liter^{-1}. The initial concentration of *E. coli* cells was 1.0×10^8 CFU · ml^{-1}, and the temperature was 22°C. t, time. C, cell count.

generation requires a contribution of the surface of the material in the presence of bacteria.

Bacterial characterizations during disinfection by the Al_2O_3-TiO_2-Ag material. (i) Morphological changes to *E. coli* cells. Cells were observed by transmission electron microscopy (TEM) to visualize the morphological changes to the *E. coli* cells during silver treatment (Fig. 3). Figure 3a presents a TEM micrograph of untreated bacteria with intact cell membrane contours and a relatively uniform electron density within the cell, revealing cells as they appear under normal conditions without any treatment. Figures 3b to d show TEM micrographs of bacteria after 2, 20, and 60 min of exposure to Al_2O_3-TiO_2-Ag, respectively. After the first few minutes of disinfection with silver, significant morphological changes to the shape and integrity of the *E. coli* cells, which underwent lysis or an increase in permeability, resulting in leakage of the intracellular compounds, occurred (Fig. 3b to d). Even though some intact cells were still present at the end of the disinfection, they may have been permanently inactivated, as no viable cells were enumerated at the end of the treatment (Fig. 1), and no regrowth was apparent. It is also worth noting that the degradation state of the *E. coli* cells appeared to be comparable at 20 and 60 min (Fig. 3c and d, respectively).

Figures 4b to d show the cells at a magnification greater than that used for Fig. 3 after 2 min of exposure to Al_2O_3-TiO_2-Ag. As a reference, Fig. 4a provides a micrograph with a magnification greater than that used for Fig. 3 of untreated bacteria with a spherical shape and an intact cell wall. Several morphological changes, such as an increased heterogeneity of the electron density of the cell cytoplasm, were observed. Some vacuoles corresponding to empty clear regions where the electron density was reduced were visible inside treated bacteria (Fig. 4b and c). There was also a large accumulation of electrons around the clear regions, appearing as dark regions and corresponding to zones with high electron densities (Fig. 4b and c).

Detachment of the cytoplasmic membrane from the cell wall or disruption of the cytoplasm, which could induce an increase in *E. coli* membrane permeability, is visible in Fig. 4b and c. These alterations to the cytoplasm often occurred with vacuoles. Moreover, the cells showed distorted morphologies (Fig. 4b and c), with some empty cells resulting from probable lysis (Fig. 4b). Damage to the cell wall with the partial or total disappearance of the outer membrane was also observed (Fig. 4d). These morphological changes may have led to an inability of the bacteria to maintain the membrane structure in the presence of Al_2O_3-TiO_2-Ag and, thus, to cell lysis.

(ii) Characterization of cell membrane state. In this section, damaged cells (as opposed to intact cells) refer to lysed cells that no longer had cell membranes or permeable cells that had damaged cell membranes. Intact cells are also referred to as whole cells, nonpermeable cells, or integer cells.

(a) Evaluation of cell integrity. Depending on the integrity of the cell, DNA can be confined within the cell or free in suspension. In this section, the proportion of damaged cells was obtained from the difference between the concentration of total DNA (measured by qPCR) and the concentration of DNA contained in intact cells (measured by vPCR).

Initially (at time zero), a difference of 1 log unit between the total amount of DNA and the amount contained in nonpermeable cells was noticed, as shown in Fig. 5. This contrast could be inherent to the suspension preparation, as control experiments without the study material showed that the cultivable bacterial concentra-

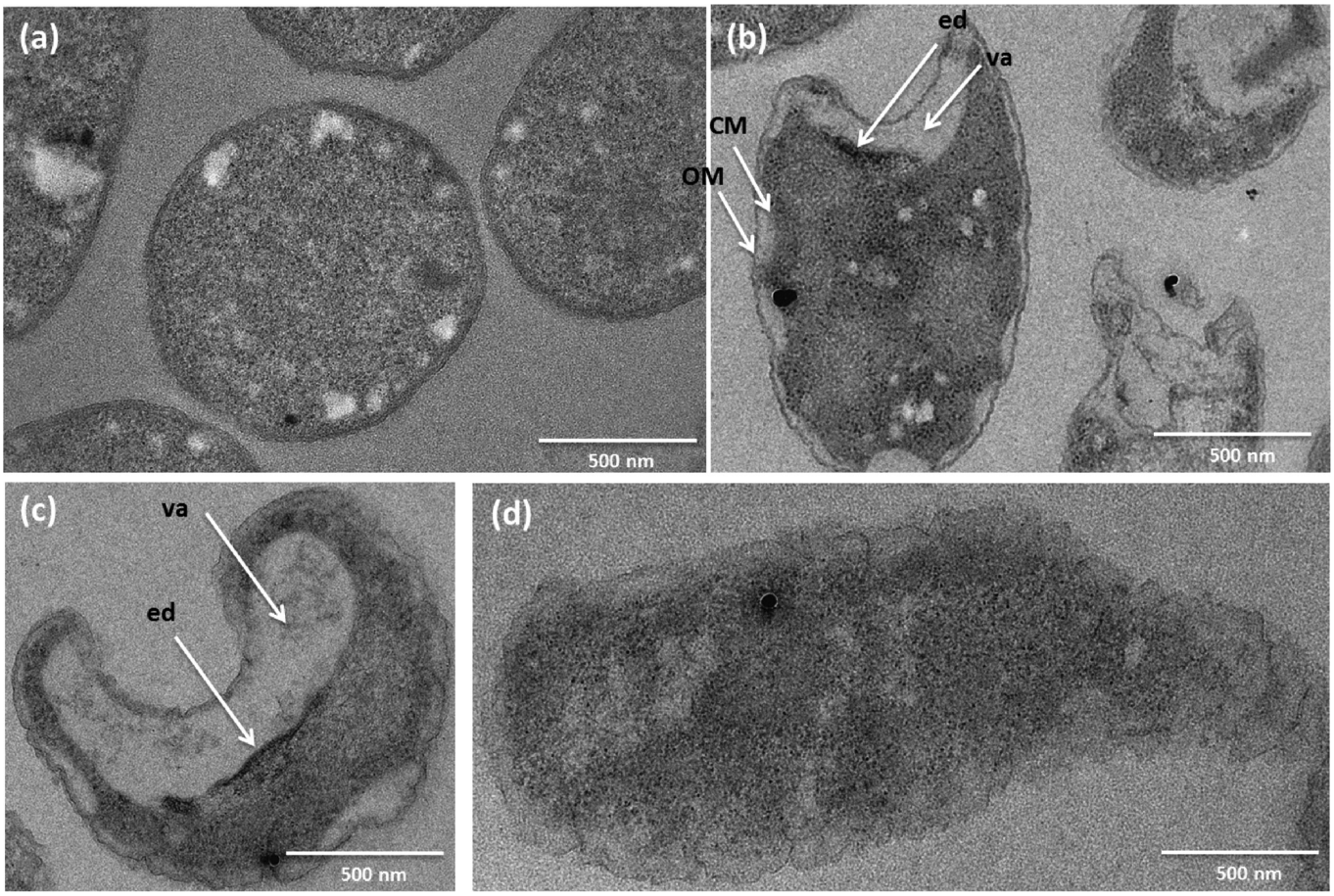

FIG 4 TEM micrographs of *E. coli* internal structures: untreated bacteria (a) and bacteria after 2 min of treatment (b to d). OM, outer membrane; CM, cytoplasmic membrane; ed, high-electron-density zone; va, vacuoles.

tion remained constant (at $1.5 \times 10^7 \pm 0.5 \times 10^7$ CFU · ml^{-1}) over 60 min (data not shown).

The results (Fig. 5) show that during the kinetics assay the total DNA content was constant at 8 log(GU · ml^{-1}), which corresponds to the initial inoculum of 10^8 CFU · ml^{-1}. In comparison, the DNA concentration of whole cells underwent a decrease of 2 log units from 6.6 to 5.2 log(GU · ml^{-1}) during the first few minutes of the action of the Al_2O_3-TiO_2-Ag material and then stabilized at 5 log(GU · ml^{-1}). It was noted that total removal of the bacteria ($1.0 \times 10^8 \pm 0.2 \times 10^8$ CFU · ml^{-1}) was reached at 45 min without any regrowth (Fig. 1). Consequently, the 5 log(GU · ml^{-1}) of intact cells (i.e., 1% of the total initial intact bacterial population) that remained constant from 30 to 60 min may correspond to noncultivable bacteria that were inactivated by the Al_2O_3-TiO_2-Ag material without significant cell damage.

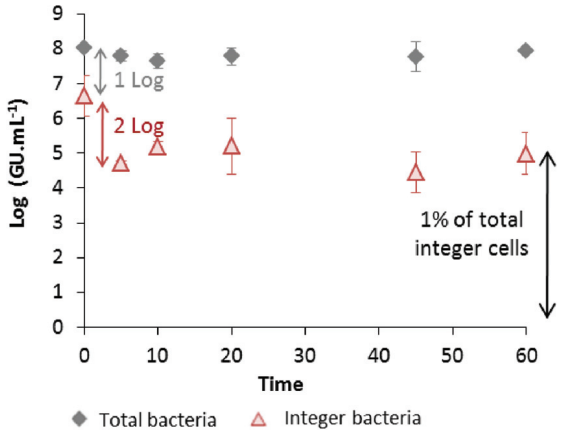

FIG 5 Change of the concentration of intact bacteria versus time during bactericidal treatment with Al_2O_3-TiO_2-Ag. Integer bacteria refers to intact cells.

From these results, it can be concluded that cell lysis occurs as soon as the treatment (i.e., direct exposure of the bacteria to the material) begins. Additional analyses conducted by flow cytometry completed the characterization of the permeability state of the cells.

(b) Evaluation of cell permeability. Figure 6 presents the change of cell permeability during the bactericidal treatment, distinguishing nonpermeable cells (i.e., undamaged cells in green) from permeable cells still having a cell membrane (in red); lysed cells were not visible by this technique. Green cells are commonly called "live cells," even though they may no longer be viable, and red cells are usually called "dead cells," even though they still have a membrane. Figures 6a and b present the findings for control cells that mainly have damaged membranes (90% of events present red fluorescence) and that predominantly have intact membranes (85%

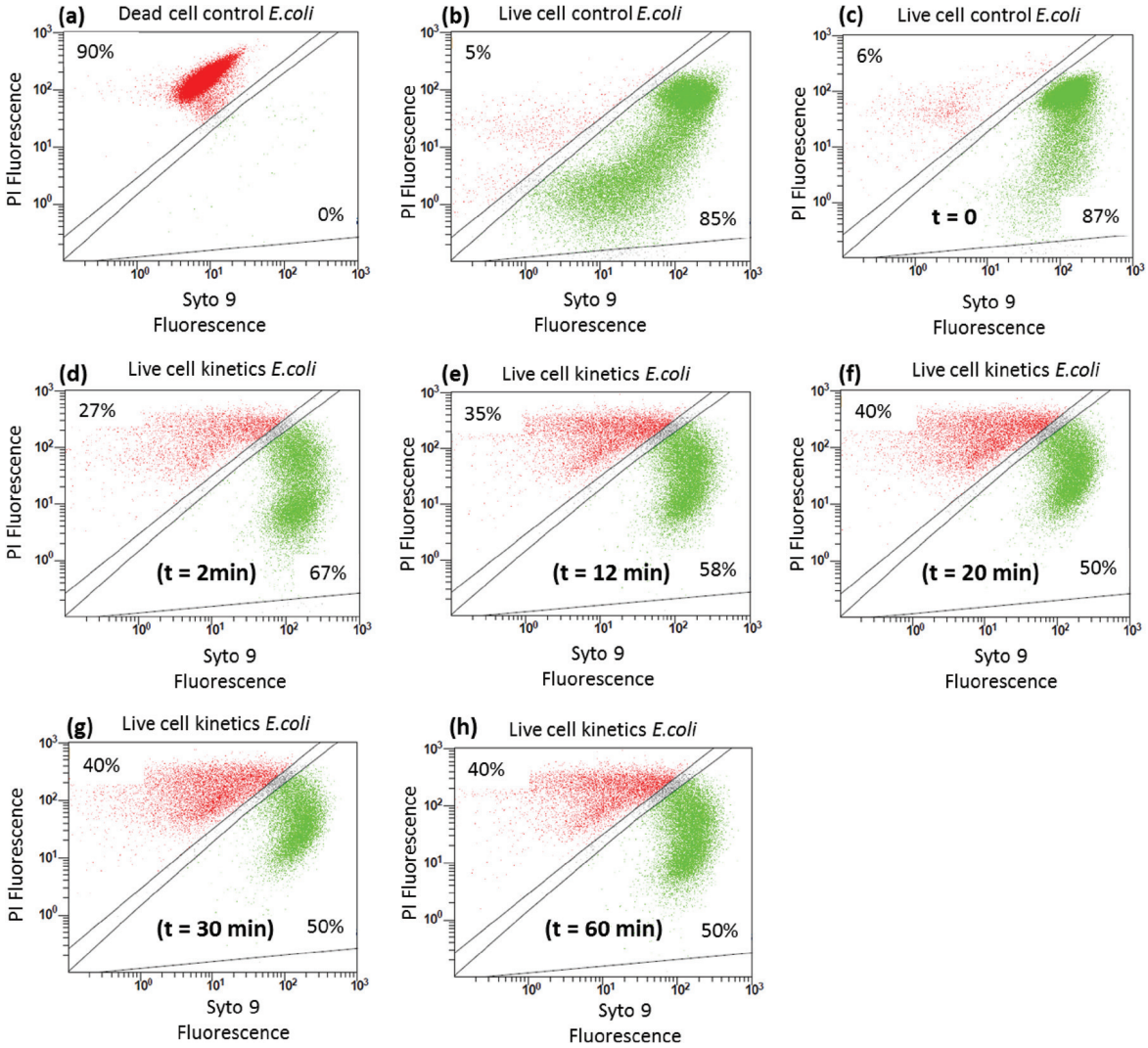

FIG 6 Change of ratio of intact cells to permeable cells during treatment with Al_2O_3-TiO_2-Ag. (a) Damaged *E. coli* cell control; (b) intact *E. coli* cell control; (c) *E. coli* cells before treatment (time zero); (d) *E. coli* cells after 2 min of treatment; (e) *E. coli* cells after 12 min of treatment; (f) *E. coli* cells after 20 min of treatment; (g) *E. coli* cells after 30 min of treatment; (h) *E. coli* cells after 60 min of treatment. PI, propidium iodide.

of events present green fluorescence), respectively. Figures 6c to h show the evolution of the relative proportions between intact bacteria and permeable cells during the bacterial treatment with the study material. Initially, 87% intact cells and 6% permeable cells were detected, probably because of the change of medium (from the culture medium to spring water), as was observed for the PCR analysis. From the first minutes of treatment, the percentage of intact cells decreased from 87% to 67% ± 8% and then reached a constant value of 50% ± 8% (Fig. 6c to h). The increase of cell permeability suspected from the TEM micrographs was confirmed by these results and occurred, as for PCR results, from the beginning of the disinfection, as soon as the bacteria were exposed to the material.

The PCR results demonstrated that 1% (1×10^5 GU · ml^{-1}) of bacteria appeared to be remain intact at the end of the disinfection, although they were permanently deactivated (Fig. 5). Flow cytometry showed that there were areas with as many intact bacteria as permeable cells at the end of the treatment. These results consequently suggest that, at the end of the disinfection period, the bacterial population was composed of 1% inactivated intact cells, 1% permeable cells, and 98% lysed cells.

DISCUSSION

TEM micrographs showed cytoplasm detachment from the cell wall and the appearance of an increasing number of vacuoles in the cell cytoplasm from 2 to 60 min of treatment (Fig. 3 and 4). It has been reported in the literature that these regions of low electron density result from the condensation of DNA molecules in their centers and zones of condensed DNA consequently become regions of high electron density. It was suggested that these phenomena could be a possible defense mechanism of bacteria against silver attack (11). The penetration of silver ions inside the cells due to an increase in cell permeability may indeed lead the DNA to condense, triggering the inhibition of bacterial growth and, consequently, inducing cell death. When DNA is in a relaxed state, it can replicate effectively, but when the DNA is in a condensed form, it loses its replication ability (16, 22). DNA condensation

due to desorbed silver is thus likely to occur during treatment with the Al_2O_3-TiO_2-Ag material.

Moreover, large amounts of electrons surrounding the regions with the lowest electron density were observed (Fig. 4b and c). Similar observations have been reported in the literature, attributing this phenomenon to the presence of sulfur and silver in these regions (11). It has been suggested that silver ions could react with protein thiol groups (—SH) to form S-Ag, which would inhibit enzyme activity and thus block the respiration process (12, 13) and electron and/or proton transfer, which could explain the accumulation of large amounts of electrons in this zone. Leakage of the respiration chain is, consequently, another mechanism that may be due to the action of desorbed silver during disinfection with the Al_2O_3-TiO_2-Ag material.

In addition to the mechanisms mentioned so far, cell membrane and cell wall decomposition could also be due to the catalytic oxidation of reactive oxygen species (ROS) (17, 23).

ROS could also interact with other cell components, such as proteins and DNA (19, 24), and trigger the destruction of the cell wall of the bacteria to cause complete lysis (16, 17). A previous study demonstrated that oxygen is required for the optimal bactericidal activity of this Al_2O_3-TiO_2-Ag material (21). In particular, a reduction of only 3.5 ± 0.9 log units of *E. coli* (in a mixture with *S. epidermidis*) was achieved under anaerobic conditions after 60 min of treatment with 16 g · liter^{-1} of material; in comparison, the total removal of 8 ± 0.9 log units occurred under aerated conditions. This phenomenon suggests the presence of ROS under aerated conditions, and ROS require the presence of oxygen for their formation.

The presence of extracellular ROS was confirmed in this study (Fig. 2). The present work showed that both bacteria and supported silver were required to form ROS, probably due to the facts that bacteria are a source of electrons necessary for oxygen (O_2) reduction and that O_2 needs to be adsorbed at the material surface to be activated (16–18). Different ROS can be generated from O_2, with the possible main reconversion of $O_2^{-\cdot}$, H_2O_2, and $OH^{\cdot}$, as described in equations 1 to 4 below, being seen (25). The production of ROS thus suggests a direct bactericidal action of the supported silver material on the cell membranes.

$$O_2 + e^- \rightarrow O_2^{-\cdot} \quad (1)$$

$$O_2^{-\cdot} + e^- + 2H^+ \rightarrow H_2O_2 \quad (2)$$

$$H_2O_2 + e^- \rightarrow OH^- + OH^{\cdot} \quad (3)$$

$$OH^- + OH^{\cdot} + e^- + 2H^+ \rightarrow 2H_2O \quad (4)$$

All these results, combined with the kinetic profiles of both desorbed silver and ROS that did not evolve strictly symmetrically with the removal of the bacteria (Fig. 1 and 2), indicate that the strong bactericidal activity of the Al_2O_3-TiO_2-Ag material is due to a synergic action of desorbed silver and supported silver (via ROS generation). These characterizations provide evidence that silver and ROS attack the cell membranes and oxidize the intracellular components after their penetration. Cell damage as a consequence of these attacks was observed. Among this damage was cytoplasm detachment, vacuole formation, cell lysis, an increase in cell permeability, and the appearance of regions with low and high electron densities (probably due to DNA condensation).

In conclusion, the bactericidal mechanisms of a silver-supported material (Al_2O_3-TiO_2-Ag) during the disinfection process were determined by the coupling of physicochemical and biomolecular analyses. This study provides evidence that the actions of both desorbed silver and ROS (generated by supported silver) are responsible for the efficient antibacterial activity of the material, while it identifies the final composition of the bacterial population. The analyses highlight that cell integrity is altered from the first minutes of treatment with the Al_2O_3-TiO_2-Ag material, leading to approximately 1% intact cells that were permanently inactivated, 1% permeable cells, and 98% lysed cells after 60 min of treatment.

ACKNOWLEDGMENTS

We are grateful to C. Duperray (Montpellier RIO Imaging, Montpellier, France), V. Richard and M. Godiard (Montpellier II University, Montpellier, France), and C. Clerte (Center for Structural Biochemistry, Montpellier, France) for their help with the flow cytometry, TEM, and fluorescence measurements. We also thank S. Becker for English language editing.

REFERENCES

1. **Hamidin N, Yu QJ, Connell DW.** 2008. Human health risk assessment of chlorinated disinfection by-products in drinking water using a probabilistic approach. Water Res **42:**3263–3274. http://dx.doi.org/10.1016/j.watres.2008.02.029.
2. **Peng JJY, Botelho MG, Matinlinna JP.** 2012. Silver compounds used in dentistry for caries management: a review. J Dent **40:**531–541. http://dx.doi.org/10.1016/j.jdent.2012.03.009.
3. **Windler L, Height M, Nowack B.** 2013. Comparative evaluation of antimicrobials for textile applications. Environ Int **53:**62–73. http://dx.doi.org/10.1016/j.envint.2012.12.010.
4. **Davies RL, Etris SF.** 1997. The development and functions of silver in water purification and disease control. Catal Today **36:**107–114. http://dx.doi.org/10.1016/S0920-5861(96)00203-9.
5. **US Environmental Protection Agency.** 2012. 2012 edition of the drinking water standards and health advisories. Report 822-S-12-001. Office of Water, US Environmental Protection Agency, Washington, DC.
6. **Matsumura Y, Yoshikata K, Kunisaki S, Tsuchido T.** 2003. Mode of bactericidal action of silver zeolite and its comparison with that of silver nitrate. Appl Environ Microbiol **69:**4278–7281. http://dx.doi.org/10.1128/AEM.69.7.4278-4281.2003.
7. **De la Rosa-Gomez I, Olguín MT, Alcántara D.** 2008. Bactericides of coliform microorganisms from wastewater using silver-clinoptilolite rich tuffs. Clay Sci **40:**45–53. http://dx.doi.org/10.1016/j.clay.2007.07.001.
8. **Chen M, Yan L, He H, Chang Q, Yu Y, Qu J.** 2007. Catalytic sterilization of *Escherichia coli* K 12 on Ag/Al_2O_3 surface. J Inorg Biochem **101:**817–823. http://dx.doi.org/10.1016/j.jinorgbio.2007.01.008.
9. **Sondi I, Salopek-Sondi B.** 2004. Silver nanoparticles as antimicrobial agent: a case study on *E. coli* as a model for Gram-negative bacteria. J Colloid Interface Sci **275:**177–182. http://dx.doi.org/10.1016/j.jcis.2004.02.012.
10. **Sintubin L, De Gusseme B, Van der Meeren P, Pycke BF, Verstraete W, Boon N.** 2011. The antibacterial activity of biogenic silver and its mode of action. Appl Microbiol Biotechnol **91:**153–162. http://dx.doi.org/10.1007/s00253-011-3225-3.
11. **Feng QL, Wu J, Chen GQ, Cui FZ, Kim TN, Kim JO.** 2000. A mechanistic study of the antibacterial effect of silver ions on *Escherichia coli* and *Staphylococcus aureus*. J Biomed Mater Res **52:**662–668. http://dx.doi.org/10.1002/1097-4636(20001215)52:4<662::AID-JBM10>3.0.CO;2-3.
12. **Liau SY, Read DC, Pugh WJ, Furr JR, Russell AD.** 1997. Interaction of silver nitrate with readily identifiable groups: relationship to the antibacterial action of silver ions. Lett Appl Microbiol **25:**279–283. http://dx.doi.org/10.1046/j.1472-765X.1997.00219.x.
13. **Holt KB, Bard AJ.** 2005. Interaction of silver(I) ions with the respiratory chain of *Escherichia coli*: an electrochemical and scanning electrochemical microscopy study of the antimicrobial mechanism of micromolar Ag^+. Biochemistry **44:**13214–13223. http://dx.doi.org/10.1021/bi0508542.
14. **Dibrov P, Dzioba J, Gosink KK, Hase CC.** 2002. Chemiosmotic mechanism of antimicrobial activity of Ag^+ in *Vibrio cholerae*. Antimicrob Agents Chemother **46:**2668–2670. http://dx.doi.org/10.1128/AAC.46.8.2668-2670.2002.

15. **Li WR, Xie XB, Shi QS, Zeng HY, Ou-Yang YS, Chen YB.** 2010. Antibacterial activity and mechanism of silver nanoparticles on *Escherichia coli*. Appl Microbiol Biotechnol **85:**1115–1122. http://dx.doi.org/10.1007/s00253-009-2159-5.
16. **Chang Q, He H, Ma Z.** 2008. Efficient disinfection of *Escherichia coli* in water by silver loaded alumina. J Inorg Biochem **102:**1736–1742. http://dx.doi.org/10.1016/j.jinorgbio.2008.05.003.
17. **Inoue Y, Hoshino M, Takahashi H, Noguchi T, Murata T, Kanzaki Y, Hamashima H, Sasatsu M.** 2002. Bactericidal activity of Ag-zeolite mediated by reactive oxygen species under aerated conditions. J Inorg Biochem **92:**37–42. http://dx.doi.org/10.1016/S0162-0134(02)00489-0.
18. **Su HL, Chou CC, Hung DJ, Lin SH, Pao IC, Lin JH, Huang FL, Dong RX, Lin JJ.** 2009. The disruption of bacterial membrane integrity through ROS generation induced by nanohybrids of silver and clay. Biomaterials **30:**5979–5987. http://dx.doi.org/10.1016/j.biomaterials.2009.07.030.
19. **Park HJ, Kim JY, Kim J, Lee JH, Hahn JS, Gu MB, Yoon J.** 2009. Silver-ion-mediated reactive oxygen species generation affecting bactericidal activity. Water Res **43:**1027–1032. http://dx.doi.org/10.1016/j.watres.2008.12.002.
20. **Chis CV.** January 2013. Silver containing antimicrobial material and uses thereof. International patent WO/2013/007289.
21. **Tartanson MA, Soussan L, Rivallin M, Chis CV, Penaranda D, Lapergue R, Calmels P, Faur C.** 2014. A new silver based composite material for spa water disinfection. Water Res **63:**135–146. http://dx.doi.org/10.1016/j.watres.2014.06.019.
22. **Morones JR, Elechiguerra JL, Camacho A, Holt K, Kouri JB, Ramirez JT, Yacaman MJ.** 2005. The bactericidal effect of silver nanoparticles. Nanotechnology **16:**2346–2353. http://dx.doi.org/10.1088/0957-4484/16/10/059.
23. **Fauss EK, MacCuspie RI, Oyanedel-Craver V, Smith JA, Swami NS.** 2014. Disinfection action of electrostatic versus steric-stabilized silver nanoparticles on *E. coli* under different water chemistries. Colloids Surf B Biointerfaces **113:**77–84. http://dx.doi.org/10.1016/j.colsurfb.2013.08.027.
24. **Valko M, Leibfritz D, Moncol J, Cronin MTD, Mazur M, Telser J.** 2007. Free radicals and antioxidants in normal physiological functions and human disease. Int J Biochem Cell Biol **39:**44–84. http://dx.doi.org/10.1016/j.biocel.2006.07.001.
25. **Choi O, Hu Z.** 2008. Size dependent and reactive oxygen species related nanosilver toxicity to nitriafying bacteria. Environ Sci Technol **42:**4583–4588. http://dx.doi.org/10.1021/es703238h.